Monthly Notices
of the
ROYAL ASTRONOMICAL SOCIETY

Mon. Not. R. Astron. Soc. **405,** 494–502 (2010) doi:10.1111/j.1365-2966.2010.16461.x

Cosmic shear requirements on the wavelength dependence of telescope point spread functions

E. S. Cypriano,[1,2]★ A. Amara,[3] L. M. Voigt,[2] S. L. Bridle,[2] F. B. Abdalla,[2] A. Réfrégier,[4] M. Seiffert[5,6] and J. Rhodes[5,6]

[1]*Departamento de Astronomia, Instituto de Astronomia, Geofísica e Ciências Atmosféricas, Universidade de São Paulo, Rua do Matão 1226, Cidade Universitária 05508-900, São Paulo, SP, Brazil*
[2]*Department of Physics and Astronomy, University College London, Gower Street, London WC1E 6BT*
[3]*Department of Physics, ETH Zürich, Wolfgang-Pauli-Strasse 16, CH-8093 Zürich, Switzerland*
[4]*Service dÁstrophysique, CEA Saclay, 91191 Gif sur Yvette, France*
[5]*Jet Propulsion Laboratory, California Institute of Technology, 4800 Oak Grove Drive, Pasadena, CA 91109, USA*
[6]*California Institute of Technology, 1201 E California Blvd., Pasadena, CA 91125, USA*

Accepted 2010 February 1. Received 2010 January 29; in original form 2010 January 5

ABSTRACT

Cosmic shear requires high precision measurement of galaxy shapes in the presence of the observational point spread function (PSF) that smears out the image. The PSF must therefore be known for each galaxy to a high accuracy. However, for several reasons, the PSF is usually wavelength dependent; therefore, the differences between the spectral energy distribution of the observed objects introduce further complexity. In this paper, we investigate the effect of the wavelength dependence of the PSF, focusing on instruments in which the PSF size is dominated by the diffraction limit of the telescope and which use broad-band filters for shape measurement.

We first calculate biases on cosmological parameter estimation from cosmic shear when the stellar PSF is used uncorrected. Using realistic galaxy and star spectral energy distributions and populations and a simple three-component circular PSF, we find that the colour dependence must be taken into account for the next generation of telescopes. We then consider two different methods for removing the effect: (i) the use of stars of the same colour as the galaxies and (ii) estimation of the galaxy spectral energy distribution using multiple colours and using a telescope model for the PSF. We find that both of these methods correct the effect to levels below the tolerances required for per cent level measurements of dark energy parameters. Comparison of the two methods favours the template-fitting method because its efficiency is less dependent on galaxy redshift than the broad-band colour method and takes full advantage of deeper photometry.

Key words: gravitational lensing – cosmology: observations – large-scale structure of Universe.

1 INTRODUCTION

Measurements of the cosmic shear signal are expected to play a leading role in furthering our understanding of our Universe, in particular the nature of dark matter and dark energy or its possible alternatives such as modifications in gravity. The gravitational lensing of light from distant galaxies by intervening mass provides a powerful insight into the growth of structure and the expansion history of the universe (for recent reviews, see Refregier 2003; Hoekstra & Jain 2008; Munshi et al. 2008).

Several planned future dark energy missions are designed with weak lensing as a primary science driver, including ground-based projects: the KIlo-Degree Survey (KIDS),[1] the Panoramic Survey Telescope and Rapid Response System (Pan-STARRS),[2] the Dark Energy Survey (DES),[3] the Large Synoptic Survey Telescope (LSST),[4] space missions *Euclid*[5] (Laureijs 2009; Refregier et al.

★E-mail: cypriano@astro.iag.usp.br

[1] http://www.astro-wise.org/projects/KIDS
[2] http://pan-starrs.ifa.hawaii.edu
[3] http://www.darkenergysurvey.org
[4] http://www.lsst.org
[5] http://www.euclid-imaging.net

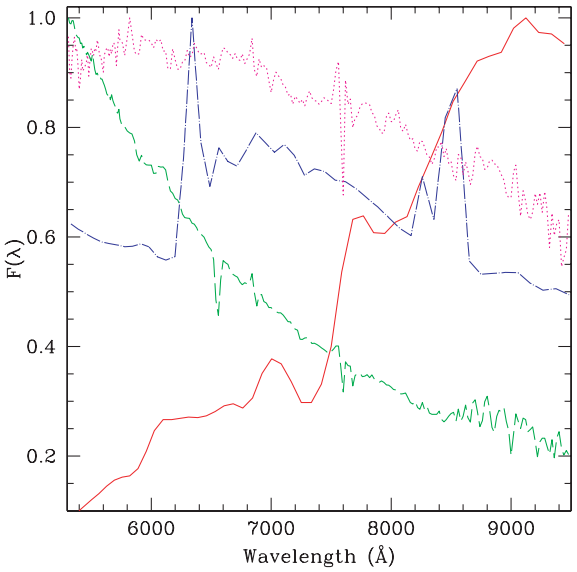

Figure 1. A sample of stellar and galaxy spectra showing the variety of SEDs among astronomical objects. An elliptical galaxy at $z = 0.9$ (solid red), an irregular galaxy at $z = 0.7$ (dot–dashed blue), an A0V star (dashed green) and a K0III star (dotted magenta).

2010) and the Joint Dark Energy Mission (JDEM).[6] The success of the method relies on accurate measurement of galaxy shapes (e.g. Heymans et al. 2006; Massey et al. 2007; Bridle et al. 2009).

As light from galaxies passes through the atmosphere, telescope optics and measurement devices it is convolved with a kernel, referred to as the point spread function (PSF). The size of the PSF is similar to the size of the galaxies used to measure cosmic shear, making accurate determination of the underlying galaxy shape a significant challenge (e.g. Lewis 2009; Voigt & Bridle 2009). Precise modelling of the PSF is crucial (e.g. Paulin-Henriksson et al. 2008). This can in principle be performed using accurate knowledge of the telescope optics; however, in practice it is usual to make use of the point-like nature of stars by modelling the PSF based on the shapes of stellar images. The situation is complicated by (i) variations in the shape of the PSF across the detector and (ii) the wavelength dependence of the PSF shape. In this paper we concentrate on the second of these two effects, focusing on a telescope which is nearly diffraction limited and on an instrument that uses broad-band optical filters for shape measurement.

Stars and galaxies have different spectral energy distributions (SEDs), both intrinsic and observed, specially if we consider that galaxies are observed over a broad range of redshifts (see Fig. 1). Therefore, the PSF shape measured from a stellar image will be different from the true PSF applied to the galaxy, leading to a bias on the measured underlying galaxy shape. The wavelength dependence of the PSF has a greater impact if observations are performed using broad-band filters. In this paper, we quantify the effect of ignoring the wavelength dependence of the PSF in a *Euclid*-like space mission and show the feasibility of reducing the effect by using colour information. We determine the wavelength dependence of the PSF shape using a simple model for the convolution kernel and applying realistic galaxy and stellar SEDs.

For the reasons we will discuss in the following sections, this paper will focus on the wavelength dependence of the PSF size. There are several measures of this quantity, such as the 50we adopt the full width at half-maximum (FWHM) intensity as our size parameter given that this is a more familiar quantity to the astronomical community and describes well the simple PSF models we use in this paper.

This paper is organized as follows. In Section 2, we set out a formalism for propagating a mis-estimation of the PSF shape through to biases on cosmological parameters. In Section 3 we describe the separate contributions to the PSF model, and in Section 4 we predict the range in PSF sizes expected for two different broad-band filters using a realistic distribution of stellar and galaxy SEDs and investigate two different methods for reducing the bias. These involve using (i) galaxy and stellar colours to correct the PSF size and (ii) template fitting. Also, we place requirements on a simple model for the wavelength dependence for a *Euclid*-like survey. Finally, in Section 5 we discuss our findings.

2 IMPLICATIONS OF USING AN INCORRECT PSF

We first make a simple calculation of the shear bias induced by mis-estimating the size and ellipticity of the PSF and compare it to the general systematics limit calculated in Amara & Réfrégier (2007). We then consider the redshift dependence of the shear biases and propagate this through to biases on cosmological parameters.

The shear measurement bias caused by an incorrect PSF will depend on the shear measurement method employed. For simplicity, we assume here that shears are calculated using unweighted quadrupole moments. Although this method is not feasible in practice due to the low signal-to-noise ratio level in real images, it is related to the widely used Kaiser, Squires and Broadhurst method (Kaiser, Squires & Broadhurst 1995). It has the advantage of being extremely easy to use for shear measurement bias calculations.

Shear mis-estimates are often quantified by Taylor expanding the estimated two-component shear $\hat{\gamma}_i (i = 1, 2)$ in terms of the true shear γ_i as

$$\hat{\gamma}_i = m_i \gamma_i + c_i, \tag{1}$$

where m_i is referred to as the multiplicative bias, c_i as the additive bias (Heymans et al. 2006) and it is often assumed $m_1 \simeq m_2 \equiv m$ and $c_1 \simeq c_2 \equiv c$.

Amara & Réfrégier (2007) showed that for a full-sky survey (2×10^4 deg^2 of extragalactic sky) with 35 galaxies per arcminute^2 and a median redshift of 0.9, the shear multiplicative error m must be $< 1 \times 10^{-3}$ to keep systematic biases on cosmological parameters below random uncertainties, for a range of possible redshift evolution scenarios for m. Using the equations in Appendix A, this translates to a requirement on the PSF size mis-estimate $\delta F_{\rm PSF}$ of

$$\frac{\delta F_{\rm PSF}}{F_{\rm PSF}} \simeq m \leq 1 \times 10^{-3}. \tag{2}$$

Amara & Réfrégier (2007) also placed a requirement on the mean square error $\sigma^2_{\rm sys} < 10^{-7}$ for the same survey. Interpreting this as a requirement on the square of the shear measurement additive error c^2, and neglecting the subdominant term in equation (A8), this places a requirement on the PSF ellipticity mis-estimate $\delta\epsilon_{{\rm PSF}\,i}$ of

$$\delta\epsilon_{{\rm PSF}\,i} \simeq 4c \leq 1 \times 10^{-3}. \tag{3}$$

Because the observed SED of a galaxy changes with redshift, the appropriate PSF will also depend on galaxy redshift. Therefore, the PSF biases $\delta F_{\rm PSF}$ and $\delta\epsilon_{\rm PSF}$ depend on redshift and so do the multiplicative and additive biases m and c. If, for example, the impact of the multiplicative and additive biases as a function of redshift

[6] http://jdem.gsfc.nasa.gov

mimics a particular cosmological parameter, the requirements may be more stringent than the above more approximate calculation. We will therefore calculate PSF biases as a function of galaxy redshift and insert them into the more detailed calculation described below, which propagates the effect into biases on cosmological parameters.

Use of the wrong PSF model will cause the measured cosmic shear cross power spectra between redshift bins i and j, $\hat{C}^{\kappa}_{ij}(\ell)$, to differ from the true cosmic shear power spectra, $C^{\kappa}_{ij}(\ell)$. If a particular systematic on the cosmic shear power spectrum $\Delta C^{\kappa}_{ij}(\ell) = \hat{C}^{\kappa}_{ij}(\ell) - C^{\kappa}_{ij}(\ell)$ is ignored, then the bias on cosmological parameters δp_{α} is given by

$$\delta p_{\alpha} = \mathcal{F}^{-1}_{\alpha\beta} \sum_{\ell} \Delta C^{\kappa}_{ij} \left\{ \mathrm{Cov}\left[C^{\kappa}_{ij}(\ell), C^{\kappa}_{kl}(\ell)\right] \right\}^{-1} \frac{\partial C^{\kappa}_{kl}(\ell)}{\partial p_{\beta}}, \quad (4)$$

where i, j, k, l and β are summed over, $\mathrm{Cov}[C^{\kappa}_{ij}(\ell), C^{\kappa}_{kl}(\ell)]$ is the two-dimensional covariance matrix between the cross-spectra and $\mathcal{F}$ is the Fisher matrix between the cosmological parameters (Huterer et al. 2006; Amara & Réfrégier 2007). In the presence of a redshift-dependent multiplicative bias, the measured lensing power spectrum can be given in terms of the true lensing power spectrum by

$$\hat{C}^{\kappa}_{ij}(\ell) = C^{\kappa}_{ij}(\ell)(1 + m^{i} + m^{j}), \quad (5)$$

where m^{i} is the multiplicative bias for redshift bin i, averaged over all galaxies (Huterer et al. 2006, equation 16).

The impact of additive errors depends to first order on the spatial variation of the additive errors. For the case of a wavelength-dependent PSF, this will induce power on the scale of the separation between stars of a typical colour, which may be propagated into cosmology (see also Guzik & Bernstein 2005). Here we focus on PSF size mis-estimates and therefore do not consider additive errors further.

In this paper we compare the PSF sizes for stars with those for galaxies, without considering the galaxy morphology or profile. The equations derived above and in Appendix A make it possible to draw significant conclusions about the cosmology biases independent of considerations about the galaxy light distribution, if all parts of the galaxy have the same colour. Our main metric is the difference between the FWHM of the stellar and galaxy PSFs. We average this over populations of galaxies for various different PSF correction schemes.

3 THE PSF MODEL

We consider a simple instrument model in which the PSF is made up of three circular components, each with a different wavelength dependence. This is reasonable for a space-based instrument composed mainly of reflective surfaces, such as *Euclid*. For such an instrument the PSF ellipticity is relatively insensitive to wavelength, and the three main PSF components are (i) nearly diffraction-limited telescope optics giving rise to an Airy disc with a size inversely proportional to the wavelength (ii) the CCD modulation transfer function (MTF) which tends to spread out higher energy photons more than lower energy photons and (iii) a wavelength-independent part such as telescope jitter. We assume for simplicity that each component is Gaussian with a wavelength-dependent size.

We describe the total size of the PSF by its FWHM, F, which is given by the quadratic sum of the FWHM values of the three components:

$$F^{2}_{\mathrm{PSF}}(\lambda) = F^{2}_{\mathrm{D}}(\lambda) + F^{2}_{\mathrm{MTF}}(\lambda) + F^{2}_{\mathrm{J}}. \quad (6)$$

Note that the addition in quadrature works reasonably well even if the diffraction-limited component is not a Gaussian: we find that adding FWHMs in quadrature works to better than 5 per cent accuracy when an Airy disc is convolved with a Gaussian of the same FWHM and improves to better than 2 per cent accuracy if the ratio of FWHMs is changed by a factor of 4 either way.

The size of the diffraction-limited image is given by

$$F_{\mathrm{D}}(\lambda) = 0.154\,\mathrm{arcsec} \left(\frac{D}{1.2\,\mathrm{m}}\right)^{-1} \left(\frac{\lambda}{7350\,\text{Å}}\right), \quad (7)$$

where D is the diameter of the primary mirror. We take the contribution from the CCD MTF to be that measured empirically for an e2v CCD 231-84 (Cropper, private communication), which is given approximately by

$$F_{\mathrm{MTF}}(\lambda) = \begin{cases} 0.11 - 0.027\,\mathrm{arcsec}\left(\frac{\lambda}{7000\,\text{Å}}\right) & \text{if } \lambda \leq 7000\,\text{Å} \\ 0.09 - 0.007\,\mathrm{arcsec}\left(\frac{\lambda}{7000\,\text{Å}}\right) & \text{if } \lambda > 7000\,\text{Å}. \end{cases} \quad (8)$$

Finally, we take the contribution to the PSF size from the achromatic component to be

$$\mathrm{FWHM_J} = 0.08\,\mathrm{arcsec} \quad (9)$$

as appropriate for a *Euclid*-like instrument.

We plot the three contributions to the PSF image size in Fig. 2 for a 1.2-m primary mirror. The image size is dominated by the diffraction limit of the instrument. Assuming that the PSF contributions from different wavelengths all have the same centroid, we can calculate the FWHM of the composite PSF from the FWHM of each component and the transmitted flux $S(\lambda)T(\lambda)$, where $S(\lambda)$ is the SED of the object and $T(\lambda)$ is the instrumental plus filter

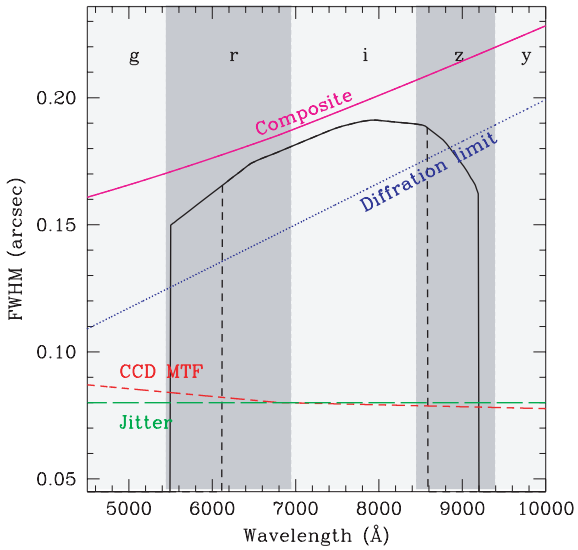

Figure 2. Contribution from each component of the PSF to the image quality (FWHM) as a function of wavelength. The dotted (blue) line represents the diffraction component, the long-dashed (red) line the CCD MTF component, the short-dashed (green) line the achromatic component and the thick-solid (magenta) line shows the overall result taking into account all the previously described components. The solid (black) line shows the relative instrumental passband using a wide optical filter $F1$ such as that proposed for *Euclid*. The dashed (black) vertical lines show an alternative, narrower, lensing filter ($F4$). The background shaded areas show approximately the wavelength coverage of the g, r, i, z, y filters.

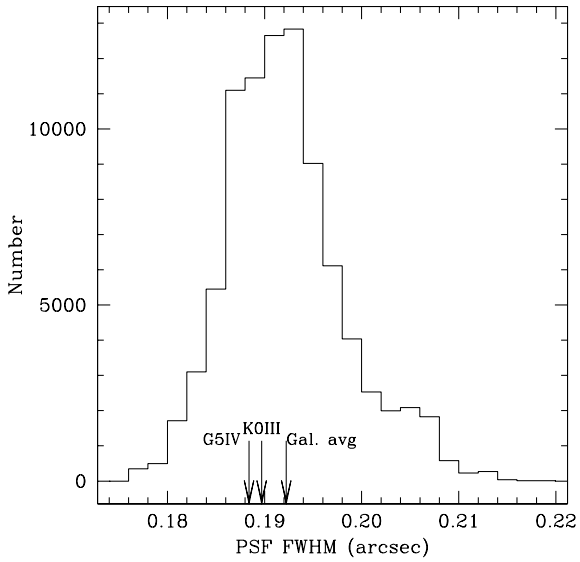

Figure 3. Histogram of the predicted PSF sizes (FWHM) for the mock galaxy catalogue. The average value of the distribution is marked on the plot with an arrow, as well as the sizes for typical disc and halo stars G5IV and K0III.

response, by

$$F^2_{\rm PSF} = \frac{\int S(\lambda)\, T(\lambda)\, F^2_{\rm PSF}(\lambda)\, {\rm d}\lambda}{\int S(\lambda)\, T(\lambda)\, {\rm d}\lambda}. \quad (10)$$

In this paper, we assume that $T(\lambda)$ is the instrumental response for the case where a wide optical $F1$ filter (5500–9200 Å; see Fig. 2) is used for measuring the shapes of galaxies, as proposed for the *Euclid* satellite.

4 PSF AND COSMOLOGY BIASES

We use realistic galaxy and stellar populations to quantify the amount by which the PSF FWHM is likely to be mis-estimated. Galaxy SEDs are generated using mock catalogues designed to simulate the distribution of redshifts, colours and magnitudes of galaxies in Great Observatories Origins Deep Survey-North (Cowie et al. 2004; Wirth et al. 2004). Template spectra are taken from Coleman, Wu & Weedman (1980) and Kinney et al. (1996) and intermediate types obtained by linear interpolation of these templates (for further details, see Abdalla et al. 2008). In this paper, we include galaxies up to a redshift of 2. Galaxies more distant than this will have small apparent sizes and are thus unlikely to be used to measure cosmic shear. For instance, for the Cosmos survey, much less than 10 per cent of the lensing usable galaxies have $z > 2.0$ (Leauthaud et al. 2007). The PSF sizes for stars are estimated using stellar SEDs from the Bruzual–Persson–Gunn–Stryker (BPGS) Spectrophotometric Atlas.[7] The catalogue contains 175 different SEDs covering a broad range of spectral types. The true PSF size for each of the star and galaxy types in the mock catalogues is then estimated by inserting its SED into equation (10).

A histogram of the FWHM distribution for the galaxy population is shown in Fig. 3. The PSF size ranges from approximately 0.175 to 0.220 arcsec, has an average of 0.1922 arcsec and a dispersion of 0.006 arcsec, or 3 per cent of the mean PSF size. As an example, the FWHM of a G5 subgiant star (taken here as a typical disc star) is typically 0.1884 arcsec, whereas a K0 giant star (typical halo/bulge star) is typically 0.1897 arcsec. In a conventional analysis which ignores the wavelength dependence of the PSF, galaxies with small angular separations from the above two example stars will often have their shears underestimated. In fact, out of all the stars in the BPGS catalogue only a quarter of them (cold K and M stars) have PSF estimated sizes larger than the average of the galaxies. The multiplicative shear mis-estimates for the example G5 and K0 stars are of the order of $m \sim 3 \times 10^{-2}$ relative to the average galaxy, in clear disagreement with our requirements on the PSF size error (equation 1) and therefore we need to explore methods for mitigating the effect. Below, we describe two methods for correcting the PSF wavelength dependence using colour information.

[7] http://www.stsci.edu/hst/observatory/cdbs/astronomical_catalogs.html#bruzual-persson-gunn-stryker

Table 1. Pan-STARRS (PS1, PS2 and PS4) and DES optical photometry depths. The values quoted here correspond to AB magnitudes of 5σ detections.

Band	PS1	PS2	PS4	DES
g	24.66	25.53	26.10	25.35
r	24.11	24.96	25.80	24.85
i	24.00	24.80	25.60	25.05
z	22.98	23.54	24.10	24.65
y	21.52	22.01	22.50	22.15

Fluxes are obtained for each object in the mock catalogues for the filters $F1$, Y, J and H up to the limiting magnitudes 26.25, 24.0, 24.0 and 24.0, respectively (AB magnitudes, 5σ detections). In addition, we consider different scenarios for the complementary ground-based photometry. We assume here observations in the filters g, r, i, z and y with three different depths each, shallow, medium and deep (see Table 1). The fiducial optical depth used in this paper (medium) is chosen to correspond to a DES or Pan-STARRS-type survey with two dedicated telescopes (PS2). Shallow and deep correspond to a Pan-STARRS-type survey with one (PS1) or four (PS4) dedicated telescopes.

4.1 Broad-band colour method

Here we investigate the possibility of estimating the galaxy PSF from stars with the same broad-band colour. For this to work well, two conditions must be met: (i) there must be a good correlation between a given broad-band colour and the PSF size and (ii) this relation must be the same for both stars and galaxies, despite their potentially differing spectra. To assess the extent to which this applies for our fiducial instrument, we have plotted the PSF sizes for the galaxy and stellar populations against two different colours: $F1 - Y$, which can be fully determined by an instrument containing a single optical filter plus the Y infrared band, such as the proposed *Euclid* design; $r - F1$, which requires r-band observations which could come from the ground. The results are shown in the top two panels of Fig. 4.

It is clear from Fig. 4 that there is a positive correlation between the PSF FWHM and the colour, i.e. redder objects tend to be larger than bluer ones. This is unsurprising given that the contribution to the PSF size from the diffraction limit of the telescope is the dominant component. It is also clear that the correlation between the PSF size and the $r - F1$ colour is tighter than with the $F1 - Y$ colour. We expect this to occur because the $r - F1$ colour constrains the slope of the SED within the lensing measuring filter $F1$, whereas the $F1 - Y$ colour constrains the SED slope at redder wavelengths,

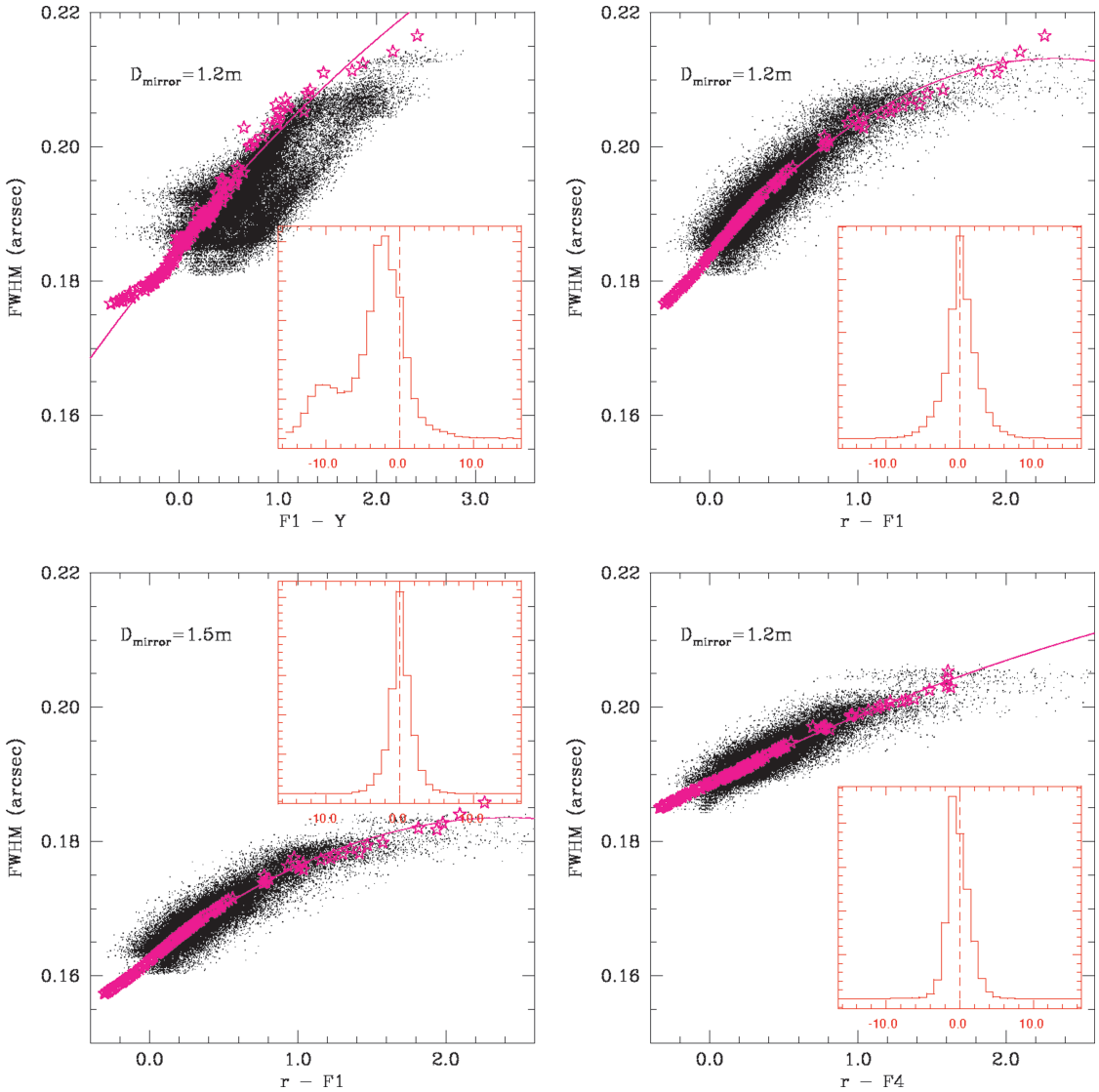

Figure 4. PSF FWHM versus colour for a realistic distribution of galaxies (black dots) and stars (magenta stars) of several different spectral types. The continuous line is a second-order polynomial fit to the stellar sequence. The insets show the residuals between the galaxy and stellar polynomial FWHM values at a given colour, in units of 10^{-3} arcsec. Results are shown using the default parameters for the mirror (1.2 m) and survey depth (medium) for the colours $F1 - Y$ (top left), $r - F1$ (top right) and $r - F4$ (bottom right; $F4$ is the shape measuring filter). The effect of using a larger mirror (1.5 m) for $r - F1$ is also shown (bottom left). $F1$ and $F4$ correspond to the wavelength ranges 5500–9200 and 6120–8580 Å , respectively.

which are less relevant. This interpretation is strengthened by the fact that other colours such as $r - z$, $g - z$ and $g - Y$, which are also able to constrain the slope of the SED over the shape measuring filter, produce correlations almost as tight as those for $r - F1$.

For the distribution of stellar SEDs used in this paper, we can see from Fig. 4 that the stars occupy a well-defined locus in the FWHM versus colour space. We fit a parabola to these data and by doing so we can estimate the PSF size from a colour alone. From the figure, we see that this line fits well through the stellar data points and thus we meet condition (i) for the stars. It is fortunate that the wavelength dependence of the PSF tends to be, to a first approximation, relatively stable. This means that it is viable to use data from several high signal-to-noise ratio stars from several different fields to empirically find this locus (provided that the wavelength-independent effects on the PSF are properly dealt with). To test condition (ii), we have to assess how well the PSF size wavelength dependence for galaxies follows that of the stars. We therefore calculate the residuals between the FWHM of the galaxies and the fit to the stellar FWHM–colour relation (shown in the insets of the figure).

The bias on the PSF size, $\langle \delta F_{\rm PSF} \rangle$, is reduced dramatically by including ground-based photometry, decreasing in magnitude from 3.6×10^{-3} arcsec for $F1 - Y$ to 0.16×10^{-3} arcsec for $r - F1$.[8] For a simple calculation in which the dependence of the multiplicative bias on redshift is not taken into account, we find from equation (2) that $\delta F_{\rm PSF}$ must be $<0.2 \times 10^{-3}$ arcsec for a typical PSF size of $F = 0.2$ arcsec. The inclusion of ground-based photometry thus allows us to meet our simple 'back-of-the-envelope' requirement (equation 2). Using a shallower r-band photometry depth

[8] Unless otherwise stated, the photometry depths are for a 'medium-depth' survey, corresponding to a PS2 survey (see Table 1 for depths in the g, r, i, z and y bands).

(PS1-like) increases the bias by a factor of 2.5 from the value with the fiducial (medium) depth. However, using a deeper ground-based photometry depth (PS4-like) has no effect on the bias. This suggests that there is an intrinsic difference between the distributions of PSF sizes for typical star and galaxy SEDs (measured in the $F1$ band) with the same $r - F1$ colour, which is not reduced by increasing the photometry depth beyond 'medium'.

The wavelength dependence of the PSF size can be reduced by increasing the size of the primary mirror (since the telescope is diffraction-limited). We find that the bias is reduced by a factor of 1.6 by increasing the mirror diameter from the fiducial value (1.2 m) to 1.5 m (see the bottom left-hand panel of Fig. 4).[9] For instance, for a space telescope, such as the *Hubble Space Telescope* (*HST*), with a 2.4 m mirror, the diffraction component will contribute the same as the CCD MTF and the jitter at ∼7500 Å. In this case, the overall optics becomes much less chromatic, in particular for bluer wavelengths where the CCD MTF partially compensates the diffraction effect. This is directly reflected in the bias we estimate as $\langle \delta F_{\rm PSF} \rangle$ becomes as small as 0.03×10^{-3} arcsec (less than five times the value of our default configuration). On the other hand, a mirror as small as 0.6 m will induce a bias in the PSF size of 0.46×10^{-3} arcsec or 2.5 times larger than the bias we obtained with the fiducial configuration.

Another way to reduce the chromaticity of the system is by using a shape measurement filter $F4$ whose passband is two-third narrower than $F1$ (see Fig. 2). By using the narrower shape measurement filter, we increased to an absolute bias value from +0.16 to −0.18 mas. As we can see in Fig. 4 (bottom right-hand panel), this configuration indeed decreases the slope of the PSF FWHM–colour relation for stars and galaxies. However, for this particular colour of choice ($r - F4$), the 'matching-up' of stars and galaxies becomes poorer. If, for instance, we use the colour $g - z$ instead we get a bias of −0.11, which captures the improvement we expected by using a narrower filter.

4.1.1 Redshift dependence

Galaxies with the same intrinsic spectra will have different observed colours as a result of the range of galaxy redshifts. The bias on the PSF FWHM is thus redshift-dependent and could potentially be very damaging to weak-lensing tomography. In the previous section, we calculated the mean bias on the PSF FWHM for the galaxy SEDs averaged over all redshifts included in the catalogue ($z < 2$). In this section, we investigate the effect of the redshift dependence of the galaxy colours.

Fig. 5 shows the redshift dependence of $\delta F_{\rm PSF}$ for the fiducial scenario (red dashed line). There is a large negative bias at high redshift which will affect a small fraction of galaxies. We also see clearly the biggest limitation of our global average method, since in this method positive and negative contributions will cancel.

We propagate this through to dark-energy-related cosmological parameters as explained in Section 2 and divide the biases on the parameter values by the statistical errors on the parameters found using the standard Fisher matrix approach, for a 20 000 deg^2 survey with 35 galaxies per arcminute^2 and a total uncertainty on each shear component of $\sigma_\gamma = 0.35$. The results are shown in Table 2.

[9] For these simulations, the changes in the instrumental configuration do not change the signal-to-noise ratio of the observations; thus, the same galaxies are observed in all cases.

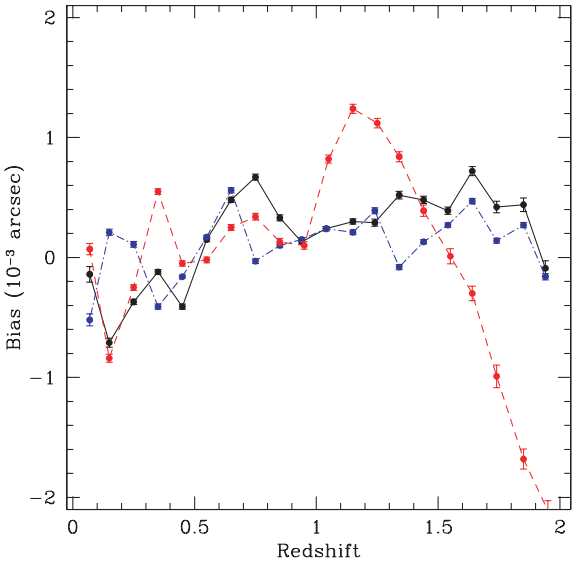

Figure 5. Residual between the actual and the best estimate galaxy PSF FWHM as a function of redshift with the broad-band method using the $r - F1$ colour (red dashed) and the template-fitting method using the shape measurement filters $F1$ (5500–9200 Å) (black solid) and $F4$ (6120–8580 Å) (blue dot–dashed).

We see that for all configurations, all the dark energy parameter biases we get are smaller than the expected statistical errors. In particular, for w_a, the most demanding parameter these surveys are trying to determine, the bias corrected by the broad-band colour method is less than a half of the statistical error level for our fiducial survey configuration. The other trends follow those already discussed in the context of the global averaged biases discussed in the beginning of this section.

4.2 Template-fitting method

The previous section assumes that we use a single colour to determine the correct PSF model to use for a given galaxy. In practice we will have more than two filters, which will be used to calculate photometric redshifts. We therefore also consider the use of a template-fitting method to predict the PSF FWHM of a galaxy by using all the colours available. Using ANNZ (Collister & Lahav 2004), we trained and validated a neural network using approximately one-third of the simulated galaxies available, to predict the redshifts, spectral types and reddening of each galaxy, given the multicolour information. With this information, we can compute the SED of each object and use a model of the PSF wavelength dependence to predict the PSF FWHM for this galaxy.

A telescope model and stars will be used to build this model for the wavelength dependence, and the accuracy of the model will depend on the stability of the wavelength dependence on telescope properties and the number of stars available to calibrate which model to use. In the case of the *HST*, a PSF model taken from the telescope design is routinely used in conjunction with calibration from any stars in the field to assess the telescope configuration in a given observation. Therefore in this paper, we use the exact model as given in equation (10) and propagate the noisy and potentially biased galaxy SED estimates through to PSF biases and cosmological parameter biases.

The comparison between this predicted PSF FWHM and the truth for the exact galaxy SED and redshift can be seen in Fig. 6.

Table 2. Biases on dark-energy-related cosmological parameters divided by the statistical uncertainty (0.035, 0.045 and 0.149 for $\Omega_{\rm DE}$, w_0 and w_a, respectively) on the cosmological parameter. Results are shown for each correction method.

Colour information	D (m)	Lensing filter	Photometry depth	$b(\Omega_{\rm DE})/\sigma(\Omega_{\rm DE})$	$b(w_0)/\sigma(w_0)$	$b(w_a)/\sigma(w_a)$
		Broad-band colour method				
$r-F1$	1.2	$F1$	Medium	−0.05	0.17	−0.47
$r-F1$	1.2	$F1$	Shallow	−0.15	0.34	−0.79
$r-F1$	1.2	$F1$	Deep	−0.05	0.17	−0.47
$r-F1$	1.5	$F1$	Medium	−0.04	0.14	−0.36
$r-F4$	1.2	$F4$	Medium	−0.10	0.35	−0.49
		Template-fitting method				
$F1, Y, J, H, g, r, i, z, y$	1.2	$F1$	Medium	0.03	0.10	−0.43
$F1, Y, J, H, g, r, i, z, y$	1.2	$F1$	Shallow	0.12	0.18	−0.72
$F1, Y, J, H, g, r, i, z, y$	1.2	$F1$	Deep	−0.02	0.06	−0.24
$F1, Y, J, H, g, r, i, z, y$	1.5	$F1$	Medium	0.02	0.07	−0.31
$F4, Y, J, H, g, r, i, z, y$	1.2	$F4$	Medium	0.01	0.07	−0.15

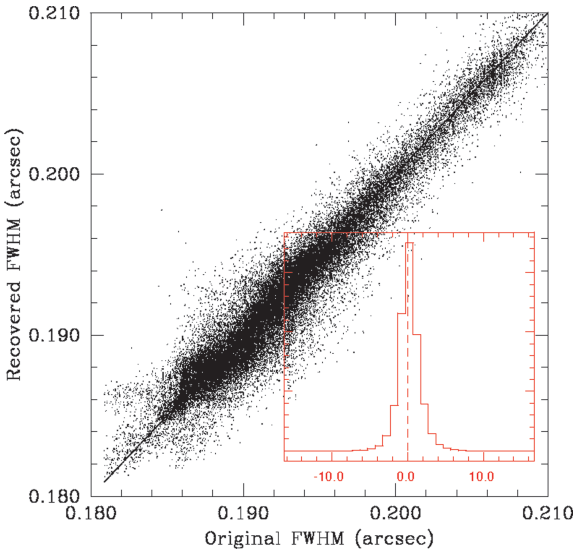

Figure 6. Comparison between the actual PSF sizes for objects with the SED of the galaxies of the mock catalogue and calculated PSF sizes given redshifts, reddening and spectral types obtained through ANNZ.

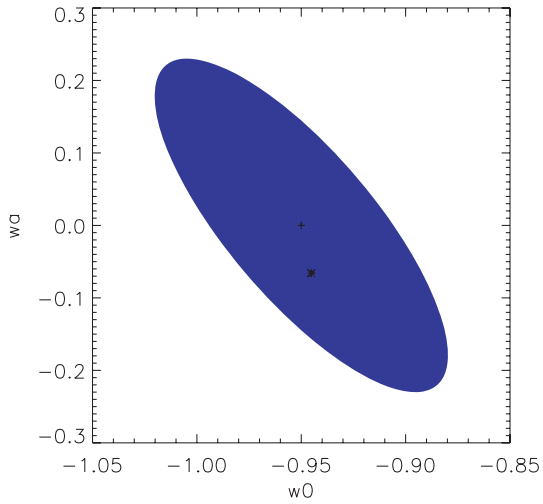

Figure 7. Bias in the dark energy equation-of-state parameters. The ellipse shows the region of the $w_0 - w_a$ space contained in the 68 per cent confidence level contour for a weak-lensing *Euclid*-type survey, where the central values are, respectively, 0.0 and −0.95 (marked by a cross). The asterisk shows the effect of the residual bias induced by the wavelength-dependence effect.

We can also compare the global averaged bias to compare with the results we got from the broad-band method and understand the trends. By using our standard configuration we obtain a bias of $\langle \delta F_{\rm PSF} \rangle = +0.19$ mas, which is similar to what we got by using one single colour and also met our 'back-of-envelope' requirement (see Fig. 6). The use of deeper photometry, a larger 1.5-m mirror or the narrower lensing filter $F4$ reduced $\langle \delta F_{\rm PSF} \rangle$ to +0.18, +0.13 and +0.12, respectively, following the expected trends.

The redshift dependence of the PSF FWHM bias is shown for the fiducial scenario (solid black line) and for a scenario with the lensing filter $F4$ (dot–dashed blue line) in Fig. 5. Both cases show much less redshift evolution than the broad-band colour method, in particular for $z > 1.0$.

We propagate this (and all the other scenarios) through into biases on cosmological parameters and find the results given in the second line of Table 2. All the biases are smaller than the statistical errors. In Fig. 7, we show the statistical confidence level uncertainties in the space $w_0 - w_a$ for our fiducial scenario. It can be seen in the figure that the residual bias after the correction of the wavelength dependence is well within the 68 per cent confidence level. In comparison to the broad-band colour method, the template-fitting method produces smaller biases on cosmological parameters and takes more advantage of the deeper photometry. In this case, by using the deepest photometry (PS4-like) we could see actual improvement when compared to the default, medium depth (PS2/DES-like).

4.3 Requirements on a simple wavelength-dependence model

Now we consider the requirements on the parameters of a simple model for PSF FWHM wavelength dependence for the template-fitting method. We approximate the FWHM–wavelength relation to be a simple linear function. The fiducial configuration is most closely approximated by a straight line whose slope is equal to 1.63×10^{-5} arcsec Å^{-1} with FWHM (7350 Å) = 0.192 arcsec. We consider a range of slopes, from a pure wavelength-independent PSF to a relation twice as steep as the fiducial configuration. In all the cases we kept the PSF FWHM constant at $\lambda = 7350$ Å, which

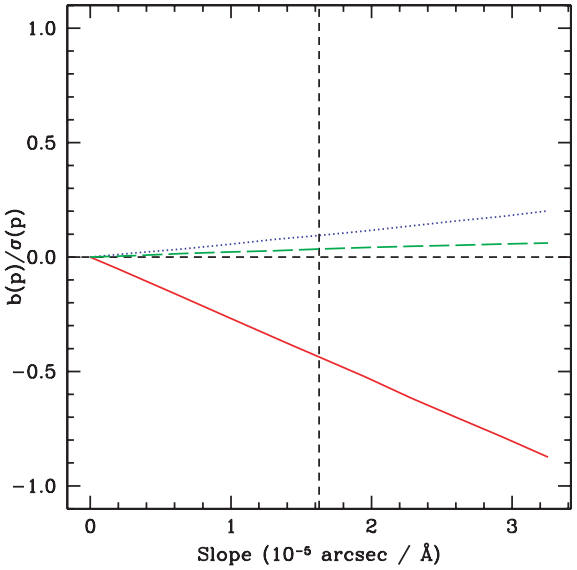

Figure 8. Variation of the systematic to statistical error ratio $[b(p)/\sigma(p)]$ of dark energy parameters as a function of the slope of the PSF FWHM–wavelength relation. The dashed (green), dotted (blue) and solid (red) lines represent the error ratio for the parameters $\Omega_{\rm DE}$, w_0 and w_a, respectively.

is the central wavelength of the lensing filters we are considering. In Fig. 8, we show the variation of the systematic to statistical error for the dark energy parameters $\Omega_{\rm DE}$, w_0 and w_a for the case where the wavelength dependence of the PSF has been corrected using the template-fitting method.

In this figure, as expected, one can see that the bias on cosmological parameters increases as the wavelength dependence of the PSF gets stronger. For all dark energy parameters, the biases lie within the region where the statistical errors are larger than the systematic ones $|b(p)/\sigma(p)| < 1$. For the evolution of the dark energy equation-of-state parameter, the normalized bias $|b(w_a)/\sigma(w_a)|$ approaches unity when the slope is double the value for the fiducial telescope mirror size and filter width.

5 DISCUSSION

The wavelength dependence of the PSF is an effect that has to be carefully considered for the next generation of cosmic shear experiments, particularly if wide bands are used for imaging. The different SEDs of stars and galaxies mean that the PSF obtained from stars is not the same as that for the galaxies, and this can lead to a non-negligible bias in shear measurements.

We have, for the first time, set out a formalism for testing the wavelength dependence of the PSF for diffraction-limited imaging, using the parameters of a *Euclid*-like survey. Given these characteristics the dominant wavelength dependence comes from the PSF size, which we parametrize by the PSF FWHM intensity. We have shown that the fractional difference in PSF FWHM between the stars and the galaxies must be smaller than 1×10^{-3}. We find the same fractional requirement on the PSF ellipticity difference. We have illustrated the formalism on a fiducial *Euclid*-like telescope for which only the PSF size is significantly wavelength dependent.

We investigated two different methods for correcting the effect and found that although they give similar results for the average PSF error, the different dependencies of the PSF size bias on redshift lead to very different implications for biases on cosmological parameters. For this type of analysis, it is therefore necessary to take into account the redshifting of galaxy spectra and the cosmological parameters of interest.

The first correction method we consider matches stars of a given colour to galaxies of the same colour. This is not expected to be a perfect correction method because the SEDs of two objects with the same colour are different. The stars and galaxies need to be matched up, so they have similar SEDs within the imaging band used for cosmic shear galaxy shape measurement. This is best achieved if the colour considered matches well to the imaging band. We find that a telescope with a wide optical band plus infrared bands cannot sufficiently self-correct for PSF wavelength dependence using the optical minus infrared colour ($F1 - Y$). This is expected because the difference in luminosity between bands so widely spaced is not well correlated with the variation in luminosity within the optical band itself. The PSF FWHM of the stars is on average 3.6×10^{-3} arcsec and a fractional error of 18×10^{-3}, much greater than our requirement (1×10^{-3}).

To realize the full potential of cosmic shear, all planned surveys will estimate the galaxy redshift using photometric redshifts. This places stringent requirements on having additional photometry in multiple wavebands, which may be obtained from the ground or from space. This provides the ideal input into correction for the wavelength dependence of the PSF. We consider the colour $r - F1$, which provides much more useful information about the SED in the $F1$ optical band. The average difference in PSF FWHM between the stars and galaxies now meets our requirement. The redshift dependence shows some evolution and tends to present larger values for redshifts larger than 1.0. However we find that the dark energy equation-of-state evolution parameter will not be biased by more than the statistical error if this method is used, even in the case where we use a shallow ground-based photometry.

We therefore consider an additional method in which the full range of available wavebands is used, to match those used in photometric redshift estimation. We take advantage of the fact that many methods for estimating the galaxy photometric redshift also provide an estimate of the galaxy SED. This allows a full model of the galaxy spectrum to be used in correcting for the PSF wavelength dependence. The extent to which this is helpful depends on how well the instrument PSF wavelength dependence is already known. We do already have a reasonable model for the wavelength dependence. Additionally we expect the wavelength dependence to be quite stable as a function of time, and furthermore it should be very well calibratable using stars. In this work we assume that the model for the wavelength dependence is therefore very well known, and the limiting factor in the analysis comes from uncertainties in the galaxy photometry, which limit our knowledge of the galaxy redshift and SED. We find for the several cases we tested that the redshift dependence of the bias is smaller, when compared to the broad-band method, and, as a consequence, the dark energy cosmological parameter biases are also smaller.

We consider the effect of a different telescope mirror size and imaging filter width. We find that the large mirror size does decrease the biases, as expected due to the smaller contribution to the wavelength dependence from the diffraction limit. The reduction is around 20 per cent for both correction methods. Using a narrower filter reduces the scatter on the PSF FWHM but does not decrease the bias, for our particular configuration.

Finally, we consider a general linear PSF wavelength dependence which matches well to the *Euclid*-like fiducial configuration. This allows a requirement on the linear slope of the PSF to be obtained for a given required accuracy on cosmological parameters. We find that, by using the template-fitting method, a survey in which the

wavelength dependence of the PSF is twice as strong as our fiducial *Euclid*-like survey just meets the requirement that $|b(p)/\sigma(p)| < 1$.

In this work, we have studied the first-order effects of a wavelength-dependent PSF and have shown that this effect can be mitigated with the addition of photometric data. The next step is to consider higher order effects such as colour gradients and the spatial correlation function of galaxy colours. These issues will be tackled and discussed in later work.

ACKNOWLEDGMENTS

We are grateful to Peter Capak for providing the code used to generate the mock photometric catalogue. We thank Mark Cropper, Jerome Amiaux, Peter Doel, Ofer Lahav, James Kingston, Steve Kent, Michelle Antonik, Stephane Paulin-Henriksson, Gary Bernstein, Tom Kitching, Alexie Leauthaud and Gary Bernstein for helpful conversations. ESC acknowledges support from FAPESP (process number 2009/07154-8). LMV acknowledges support from STFC. SLB and FBA thank the Royal Society for support in the form of a University Research Fellowship. The research described in this paper was performed in part at the Jet Propulsion Laboratory, California Institute of Technology, under a contract with the National Aeronautics and Space Administration.

REFERENCES

Abdalla F. B., Amara A., Capak P., Cypriano E. S., Lahav O., Rhodes J., 2008, MNRAS, 387, 969
Amara A., Réfrégier A., 2007, MNRAS, 381, 1018
Bridle S. et al., 2009, Ann. Applied Statistics, 3, 6
Coleman G. D., Wu C.-C., Weedman D. W., 1980, ApJS, 43, 393
Collister A. A., Lahav O., 2004, PASP, 116, 345
Cowie L. L., Barger A. J., Hu E. M., Capak P., Songaila A., 2004, AJ, 127, 3137
Guzik J., Bernstein G., 2005, Phys. Rev. D, 72, 043503
Heymans C. et al., 2006, MNRAS, 368, 1323
Hoekstra H., Jain B., 2008, Annu. Rev. Nuclear Part. Sci., 58, 99
Huterer D., Takada M., Bernstein G., Jain B., 2006, MNRAS, 366, 101
Kaiser N., Squires G., Broadhurst T., 1995, ApJ, 449, 460
Kinney A. L., Calzetti D., Bohlin R. C., McQuade K., Storchi-Bergmann T., Schmitt H. R., 1996, ApJ, 467, 38
Laureijs R., 2009, Euclid Assessment Study Report (SRE-2009)2. ESA, Noordwijk
Leauthaud A. et al., 2007, ApJS, 172, 219
Lewis A., 2009, MNRAS, 398, 471
Massey R. et al., 2007, MNRAS, 376, 13
Munshi D., Valageas P., van Waerbeke L., Heavens A., 2008, Phys. Rep., 462, 67
Paulin-Henriksson S., Amara A., Voigt L., Refregier A., Bridle S. L., 2008, A&A, 484, 67
Refregier A., 2003, ARA&A, 41, 645
Refregier A., Amara A., Kitching T. D., Rassat A., Scaramella R., Weller J., 2010, Euclid Imaging Consortium Science Book, http://www.euclid-imaging.net/
Voigt L. M., Bridle S. L., 2009, preprint (arXiv:0905.4801) (doi:10.1111/j.1365-2966.2010.16300.x)
Wirth G. D. et al., 2004, AJ, 127, 3121

APPENDIX A: MULTIPLICATIVE AND ADDITIVE SHEAR MEASUREMENT ERRORS FROM PSF MIS-ESTIMATES

We follow Paulin-Henriksson et al. (2008), who define object size R and two-component ellipticity ϵ in terms of unweighted quadrupole moments Q_{ij} as

$$R^2 = Q_{11} + Q_{22} \tag{A1}$$

$$\epsilon_1 = \frac{Q_{11} - Q_{22}}{Q_{11} + Q_{22}} \tag{A2}$$

$$\epsilon_2 = \frac{2Q_{12}}{Q_{11} + Q_{22}}. \tag{A3}$$

It is shown in Paulin-Henriksson et al. (2008) that the systematic bias on a galaxy ellipticity component $\delta\epsilon^{\rm sys}_{{\rm gal}\,i}$ can be approximated in terms of the mis-estimates of the PSF size $\delta R_{\rm PSF}$ and PSF ellipticity $\delta\epsilon_{{\rm PSF}\,i}$ as

$$\delta\epsilon^{\rm sys}_{{\rm gal}\,i} \approx \left(\frac{R_{\rm PSF}}{R_{\rm gal}}\right)^2 \left[2\left(\epsilon_{{\rm gal}\,i} - \epsilon_{{\rm PSF}\,i}\right)\frac{\delta R_{\rm PSF}}{R_{\rm PSF}} - \delta\epsilon_{{\rm PSF}\,i}\right], \tag{A4}$$

where $\epsilon_{{\rm gal}\,i}$ are the original (pre-PSF but post-shear) galaxy ellipticity components and $R_{\rm gal}$ is the galaxy size. Similar definitions apply for the PSF ellipticity and size. This assumes that the PSF and galaxy size and ellipticity measurements are made using unweighted quadrupole moments. This propagates into a bias on the shear estimate $\hat{\gamma}_i = \gamma_i + \delta\gamma_i$ as

$$\delta\gamma_i = \frac{\delta\epsilon^{\rm sys}_{{\rm gal}\,i}}{P^\gamma}, \tag{A5}$$

where P^γ is the shear responsivity given by $P^\gamma = 2 - \langle|\epsilon|^2\rangle \sim 1.8$ for simple shear measurement methods. Similarly, $\gamma_i = \epsilon_{{\rm gal}\,i}/P^\gamma$.

In this paper we quantify object sizes in terms of the slightly more intuitive quantity, the FWHM, F, where

$$F = 2\sqrt{\ln 2}\; R \tag{A6}$$

for a Gaussian profile, which we use for the PSF component in this paper. We combine equations (1), (A5) and (A6) and compare with equation (A4) to find

$$m = 2\left(\frac{R_{\rm PSF}}{R_{\rm gal}}\right)^2 \frac{\delta F_{\rm PSF}}{F_{\rm PSF}} \tag{A7}$$

$$c_i = -\frac{1}{P_\gamma}\left(\frac{R_{\rm PSF}}{R_{\rm gal}}\right)^2 \left(2\,\epsilon_{{\rm PSF}\,i}\,\frac{\delta F_{\rm PSF}}{F_{\rm PSF}} + \delta\epsilon_{{\rm PSF}\,i}\right), \tag{A8}$$

where the second term in c_i dominates for typical future surveys because $\epsilon_{{\rm PSF}\,i}$ is small, in addition to the small value of the fractional uncertainty in the PSF FWHM. We have ignored the contribution to c_i from intrinsic galaxy ellipticities, as appropriate for the case where the average c_i over randomly oriented galaxy ellipticities is required. Where useful we have converted PSF sizes into FWHM values but we have left galaxy sizes written using R since the conversion from R to F is dependent on the object profile and is far from Gaussian for galaxies. As in Paulin-Henriksson et al. (2008), we assume $R_{\rm gal} \geq 1.5R_{\rm PSF}$ and thus $R_{\rm PSF}/R_{\rm gal} \simeq 0.5$. Thus, as expected, multiplicative errors arise from errors in the PSF size and additive errors arise from errors in the PSF ellipticity.

This paper has been typeset from a TEX/LATEX file prepared by the author.